Exactly soluble two-state quantum models with linear couplings



2008 J. Phys. A: Math. Theor. 41 155309

(http://iopscience.iop.org/1751-8121/41/15/155309)

IOP PUBLISHING JOURNAL OF PHYSICS A: MATHEMATICAL AND THEORETICAL

J. Phys. A: Math. Theor. **41** (2008) 155309 (16pp) doi:10.1088/1751-8113/41/15/155309

# Exactly soluble two-state quantum models with linear couplings

**B T Torosov**[1] **and N V Vitanov**[1,2]

[1] Department of Physics, Sofia University, James Bourchier 5 blvd, 1164 Sofia, Bulgaria
[2] Institute of Solid State Physics, Bulgarian Academy of Sciences, Tsarigradsko chaussée 72, 1784 Sofia, Bulgaria

E-mail: torosov@phys.uni-sofia.bg and vitanov@phys.uni-sofia.bg

Received 11 January 2008, in final form 3 March 2008
Published 2 April 2008
Online at stacks.iop.org/JPhysA/41/155309

**Abstract**

A class of exact analytic solutions of the time-dependent Schrödinger equation is presented for a two-state quantum system coherently driven by a nonresonant external field. The coupling is a linear function of time with a finite duration and the detuning is constant. Four special models are considered in detail, namely the shark, double-shark, tent and zigzag models. The exact solution is derived by rotation of the Landau–Zener propagator at an angle of $\pi/4$ and is expressed in terms of Weber's parabolic cylinder function. Approximations for the transition probabilities are derived for all four models by using the asymptotics of the Weber function; these approximations demonstrate various effects of physical interest for each model.

PACS numbers: 32.80.Xx, 33.80.Be, 32.80.Qk, 03.65.Ge

(Some figures in this article are in colour only in the electronic version)

## 1. Introduction

In many experiments in quantum physics a two-state transition suffices to describe the essential changes in the internal state of a quantum system subjected to a generally time-dependent external field. Even when multiple states are involved, the quantum dynamics can often be understood only by reduction to one or more effective two-state systems. The coherent two-state dynamics is extensively studied, particularly in relation to nuclear magnetic resonance [1], atomic collisions [2], coherent atomic excitation [3], and most recently, as a qubit for quantum information processing [4].

On exact resonance, when the frequency of the driving field is equal to the transition frequency, the Schrödinger equation is solved exactly, for any time dependence of the coupling $\Omega(t)$ (the Rabi frequency), and the transition probability $\mathcal{P}$ depends on the pulse area $A = \int_{-\infty}^{\infty} \Omega(t)\,\mathrm{d}t$ only, $\mathcal{P} = \sin^2(A/2)$ [1–4]. Of particular use are the $\pi$ pulses,

  

which produce complete population inversion (CPI) between the two states, $2\pi$ pulses, which produce complete population return (CPR), and half-$\pi$ pulses, which create an equal coherent superposition of the two states.

There are several exactly soluble *non-resonant* two-state models, including the Rabi [5], Landau–Zener [6], Rosen–Zener [7], Allen–Eberly [8, 9], Bambini–Berman [10], Demkov–Kunike [11], Demkov [12], Nikitin [13] and Carroll–Hioe [14, 15] models. Methods for approximate solutions are also available, such as perturbation theory and the adiabatic approximation. Adiabatic evolution is of particular interest, because, when accompanied with an energy level crossing, it leads to CPI—usually referred to as rapid adiabatic passage [8, 16]. Noncrossing energies produce no excitation in the end of adiabatic evolution, i.e., CPR.

Among the exactly soluble models, the Landau–Zener (LZ) model is undoubtedly the most popular one, for it provides a very simple expression for the transition probability across a level crossing. This simplicity is somewhat surprising because the straightforward derivation uses Weber's parabolic cylinder functions, which in the end reduce to a simple exponent. (The LZ phases, though, are more complicated and involve gamma functions.) One of the unresolved mysteries of the LZ model is that despite its very simple time dependences—linearly changing energies and a constant interaction of infinite duration—it often provides much more accurate results than expected when applied to real physical systems with sophisticated time dependences. Another puzzle is that, when applied to the LZ model, various approximations, such as the Dykhne–Davis–Pechukas approximation [17] and the quasistationary adiabatic-elimination approximation [18], produce the exact result.

In this paper we use the LZ solution in a different manner: to derive a new class of exact analytical solutions to the two-state problem when the coupling is a linear function of time and the detuning is constant. Because the coupling and the detuning in our model exchange their time dependences in comparison to the LZ model, the Hamiltonians, and the respective propagators, in our model and the LZ model are connected by a basis rotation at an angle $\pi/4$. We use this rotation to derive the propagator and the transition probability for our model in terms of sums of products of Weber functions. We apply this solution to four special cases of physical interest: shark, double-shark, tent and zigzag pulses, each of which exhibits distinctive physical features. In order to reveal these features, we apply two types of asymptotics of the Weber function and derive simpler expressions in terms of elementary functions.

This paper is organized as follows. We derive the exact analytical solution of the Schrödinger equation for our general model in section 2. In sections 3–6, we present the shark, double-shark, tent and zigzag models. In section 7, we derive the respective adiabatic solutions. The conclusions are summarized in section 8.

## 2. Exact solution

The time evolution of a coherently driven two-state quantum system is described by two coupled ordinary differential equations for the probability amplitudes $C_1(t)$ and $C_2(t)$ of states $\psi_1$ and $\psi_2$,

$$\mathrm{i}\hbar\frac{\mathrm{d}}{\mathrm{d}t}\mathbf{C}(t) = \mathbf{H}(t)\mathbf{C}(t). \tag{1}$$

where $\mathbf{C}(t) = [C_1(t), C_2(t)]^T$ is a column vector with the probability amplitudes and

$$\mathbf{H}(t) = \frac{\hbar}{2}\begin{bmatrix} -\Delta(t) & \Omega(t) \\ \Omega(t) & \Delta(t) \end{bmatrix}. \tag{2}$$

In coherent atomic excitation [3], equations (1) are derived from the Schrödinger equation within the conventional rotating-wave approximation (RWA), $\Delta = \omega_0 - \omega$ is the frequency detuning between the laser carrier frequency $\omega$ and the Bohr transition frequency $\omega_0$, and $\Omega(t) = -\mathbf{d} \cdot \mathbf{E}(t)/\hbar$ is the Rabi frequency, where $\mathbf{d}$ is the transition dipole moment and $\mathbf{E}(t)$ is the laser electric-field envelope.

We shall derive the solution of equations (1) for a model, in which the coupling and the detuning are given by

$$\Omega(t) = \begin{cases} \beta^2 t & \text{for} \quad t_i \leqslant t \leqslant t_f, \\ 0 & \text{elsewhere,} \end{cases} \tag{3a}$$

$$\Delta(t) = \Delta_0, \tag{3b}$$

where $\beta$ and $\Delta_0$ are assumed positive without loss of generality (our main concern will be the transition probability, which does not depend on the signs of $\beta$ and $\Delta_0$). The turn-on time $t_i$ and the turn-off time $t_f$ can be positive, negative or zero. The model (3) resembles the exactly soluble LZ model [6], where the detuning is a linear function of time and the coupling is constant; here their time dependences are interchanged. The two models are related to each other by a basis rotation at an angle $\pi/4$ [19],

$$\widetilde{\mathbf{C}}(t) = \mathbf{R}(\pi/4)\mathbf{C}(t), \tag{4}$$

where $\widetilde{\mathbf{C}}(t) = [\widetilde{C}_1(t), \widetilde{C}_2(t)]^T$ are the probability amplitudes in the LZ model and $\mathbf{R}$ is the rotation matrix

$$\mathbf{R}(\theta) = \begin{bmatrix} \cos\theta & \sin\theta \\ -\sin\theta & \cos\theta \end{bmatrix}. \tag{5}$$

The LZ Hamiltonian reads $\widetilde{\mathbf{H}}(t) = \mathbf{R}(\pi/4)\mathbf{H}(t)\mathbf{R}(-\pi/4)$, or

$$\widetilde{\mathbf{H}}(t) = \frac{\hbar}{2} \begin{bmatrix} \beta^2 t & \Delta_0 \\ \Delta_0 & -\beta^2 t \end{bmatrix}. \tag{6}$$

The elements of the ensuing LZ propagator $\widetilde{\mathbf{U}}$ read [20]

$$\widetilde{U}_{11}(t_f, t_i) = \frac{\Gamma(1 + \mathrm{i}\delta^2)}{\sqrt{2\pi}} [D_{-\mathrm{i}\delta^2}(\alpha_f \, \mathrm{e}^{\mathrm{i}\pi/4}) D_{-1-\mathrm{i}\delta^2}(\alpha_i \, \mathrm{e}^{-3\mathrm{i}\pi/4}) + D_{-\mathrm{i}\delta^2}(\alpha_f \, \mathrm{e}^{-3\mathrm{i}\pi/4}) D_{-1-\mathrm{i}\delta^2}(\alpha_i \, \mathrm{e}^{\mathrm{i}\pi/4})], \tag{7a}$$

$$\widetilde{U}_{12}(t_f, t_i) = \frac{\Gamma(1 + \mathrm{i}\delta^2)}{\delta\sqrt{2\pi}} \, \mathrm{e}^{-\mathrm{i}\pi/4} [D_{-\mathrm{i}\delta^2}(\alpha_f \, \mathrm{e}^{\mathrm{i}\pi/4}) D_{-\mathrm{i}\delta^2}(\alpha_i \, \mathrm{e}^{-3\mathrm{i}\pi/4}) - D_{-\mathrm{i}\delta^2}(\alpha_f \, \mathrm{e}^{-3\mathrm{i}\pi/4}) D_{-\mathrm{i}\delta^2}(\alpha_i \, \mathrm{e}^{\mathrm{i}\pi/4})], \tag{7b}$$

$$\widetilde{U}_{21}(t_f, t_i) = -\widetilde{U}_{12}^*(t_f, t_i), \tag{7c}$$

$$\widetilde{U}_{22}(t_f, t_i) = \widetilde{U}_{11}^*(t_f, t_i), \tag{7d}$$

where $D_\nu(z)$ is Weber's parabolic cylinder function [21] and we have introduced the dimensionless parameters

$$\alpha_i = \beta t_i, \qquad \alpha_f = \beta t_f, \qquad \delta = \frac{\Delta_0}{2\beta}. \tag{8}$$

The parameters $\alpha_i$ and $\alpha_f$ are related to the temporal pulse areas $A_i = \alpha_i^2/2$ and $A_f = \alpha_f^2/2$, respectively, from time $t = 0$ to time $t_i$ or $t_f$.

The propagator of our system $\mathbf{U}$, defined by the relation $\mathbf{C}(t_f) = \mathbf{U}(t_f, t_i)\mathbf{C}(t_i)$, is connected to the LZ propagator $\widetilde{\mathbf{U}}$ as $\mathbf{U}(t_f, t_i) = \mathbf{R}(-\pi/4)\widetilde{\mathbf{U}}(t_f, t_i)\mathbf{R}(\pi/4)$; explicitly

$$\mathbf{U}(t_f, t_i) = \begin{bmatrix} \Re\widetilde{U}_{11} - \mathrm{i}\Im\widetilde{U}_{12} & \Re\widetilde{U}_{12} + \mathrm{i}\Im\widetilde{U}_{11} \\ -\Re\widetilde{U}_{12} + \mathrm{i}\Im\widetilde{U}_{11} & \Re\widetilde{U}_{11} + \mathrm{i}\Im\widetilde{U}_{12} \end{bmatrix}. \tag{9}$$

Therefore the transition probability is

$$\mathcal{P} = |U_{21}|^2 = (\Re\widetilde{U}_{12})^2 + (\Im\widetilde{U}_{11})^2. \tag{10}$$

Two asymptotic behaviors are of particular interest: (i) the large area and small detuning ($\alpha \gg \delta, 1$) asymptotics (to be referred to as *asymptotics I*), and (ii) the large area and large detuning ($\alpha, \delta \gg 1$) asymptotics (to be referred to as *asymptotics II*), with $\alpha = |\alpha_i|$ or $\alpha_f$. The (perturbation theory) limit of small areas ($\alpha \ll 1$) is not interesting for it produces a very small transition probability; interesting features appear for sufficiently strong fields. According to equations (7), asymptotics I requires the conventional large-argument asymptotics of the Weber function [21]. Asymptotics II requires the lesser known large-argument-and-large-order asymptotics of the Weber function, which has been derived by Olver in the general case [22]; the explicit expressions [20] for the particular Weber functions involved in the LZ model are supplied in the appendix.

We point out here that, without the basis rotation, the straightforward solution of the Schrödinger equation (1) leads to the Heun equation, and hence the propagator is expressed in terms of the Heun function; the latter is, however, much less studied than the Weber function and little is known, for instance, about its asymptotic expansions. In fact, the two approaches, with and without a basis rotation, allow one to derive interesting representations of the Heun functions as sums of products of Weber functions, unknown hitherto; this topic, however, lies outside the scope of the present paper and will be discussed elsewhere.

In the following sections we will consider four exactly soluble models of physical interest, which are special cases, or variations, of the above model. The detuning is constant in all cases and the Rabi frequencies of these models are shown in figure 1.

## 3. Shark pulse

We begin with a model in which the interaction begins at time $t_i = 0$ and ends at time $t_f = \tau > 0$, thereby forming a triangular 'shark fin' pattern, as illustrated in figure 1(*a*). By using equation (A.2) the LZ propagator elements (7) become $\widetilde{U}_{11}(\tau, 0) = a$ and $\widetilde{U}_{12}(\tau, 0) = b$, with

$$a = \frac{2^{\mathrm{i}\delta^2/2}}{2\sqrt{\pi}}\Gamma\left(\frac{1}{2} + \frac{1}{2}\mathrm{i}\delta^2\right)\left[(1 + \mathrm{e}^{-\pi\delta^2})D_{-\mathrm{i}\delta^2}(\alpha\,\mathrm{e}^{\mathrm{i}\pi/4}) - \frac{\mathrm{i}\sqrt{2\pi}}{\Gamma(\mathrm{i}\delta^2)}\,\mathrm{e}^{-\pi\delta^2/2}D_{-1+\mathrm{i}\delta^2}(\alpha\,\mathrm{e}^{-\mathrm{i}\pi/4})\right], \tag{11a}$$

$$b = \frac{2^{\mathrm{i}\delta^2/2}}{\delta\sqrt{2\pi}}\Gamma\left(1 + \frac{1}{2}\mathrm{i}\delta^2\right)\mathrm{e}^{-\mathrm{i}\pi/4}\left[(1 - \mathrm{e}^{-\pi\delta^2})D_{-\mathrm{i}\delta^2}(\alpha\,\mathrm{e}^{\mathrm{i}\pi/4}) + \frac{\mathrm{i}\sqrt{2\pi}}{\Gamma(\mathrm{i}\delta^2)}\,\mathrm{e}^{-\pi\delta^2/2}D_{-1+\mathrm{i}\delta^2}(\alpha\,\mathrm{e}^{-\mathrm{i}\pi/4})\right], \tag{11b}$$

with $\alpha = \beta\tau$. The shark propagator reads $\mathbf{U}(\tau, 0) = \mathcal{U}$, with

$$\mathcal{U} = \begin{bmatrix} \Re a - \mathrm{i}\Im b & \Re b + \mathrm{i}\Im a \\ -\Re b + \mathrm{i}\Im a & \Re a + \mathrm{i}\Im b \end{bmatrix}. \tag{12}$$

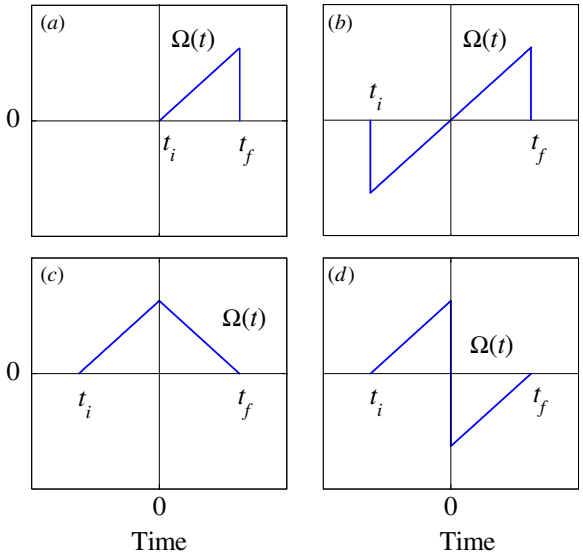


**Figure 1.** Time dependences of the Rabi frequencies of the models considered in this paper. (*a*) Shark pulse, (*b*) double-shark pulse, (*c*) tent pulse, (*d*) zigzag pulse.

We shall use this propagator $\mathcal{U}$ to express the propagators for the other three models in the following sections. The exact transition probability for the shark model is

$$\mathcal{P} = (\Im a)^2 + (\Re b)^2. \tag{13}$$

*Asymptotics I* for the transition probability is derived by using equation (A.3),

$$\mathcal{P} \sim \frac{1}{2}(1 - \mathrm{e}^{-\pi\delta^2})\cos^2\phi_1 + \frac{1}{2}(1 + \mathrm{e}^{-\pi\delta^2})\sin^2\phi_2 - \frac{\delta}{\alpha}\sqrt{1 - \mathrm{e}^{-2\pi\delta^2}}\cos(\phi_1 - \phi_2) \qquad (\alpha \gg 1, \delta), \tag{14}$$

where

$$\phi_1 = \arg\Gamma\left(1 - \frac{1}{2}\mathrm{i}\delta^2\right) + \frac{\alpha^2}{4} + \frac{\delta^2}{2}\ln\frac{\alpha^2}{2} + \frac{\pi}{4}, \tag{15a}$$

$$\phi_2 = \arg\Gamma\left(\frac{1}{2} - \frac{1}{2}\mathrm{i}\delta^2\right) + \frac{\alpha^2}{4} + \frac{\delta^2}{2}\ln\frac{\alpha^2}{2}. \tag{15b}$$

We conclude that for large $\alpha$ the transition probability oscillates versus $\alpha$ with an amplitude depending on $\delta$: for small $\delta$ ($\delta \lesssim 1$) the oscillation amplitude is large, while for large $\delta$ it decreases rapidly. These oscillations can be seen in figure 2 where the transition probability is plotted as a function of $\alpha$. The asymptotics (14) is seen to match the exact values increasingly well as $\alpha$ increases.

*Asymptotics II* for $\mathcal{P}$ is derived by using equations (A.5),

$$\mathcal{P} \sim \frac{1}{2} - \frac{\delta}{\sqrt{\alpha^2 + 4\delta^2}} \qquad (\alpha, \delta \gg 1). \tag{16}$$

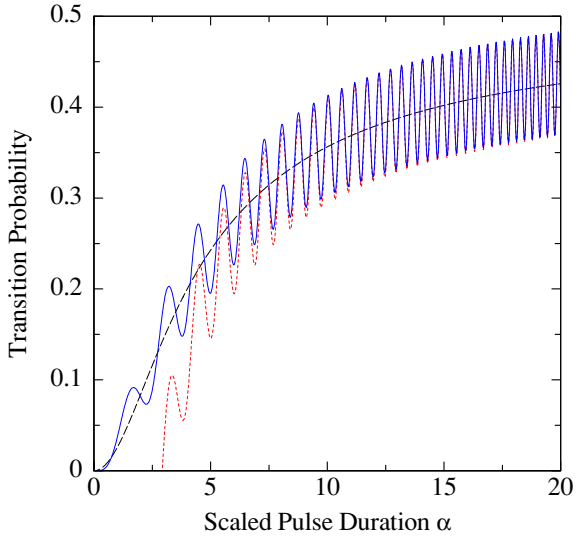


**Figure 2.** The transition probability for a *shark pulse* versus the dimensionless parameter $\alpha$ for $\delta = 1.5$. The solid curve shows the exact values (13), the short-line dashed curve shows asymptotics I (14) and the long-line dashed curve is asymptotics II (16).

This expression, and the comparison with equation (14), demonstrates that the increasing $\delta$ damps the oscillations. In the limit $\alpha \gg \delta \gg 1$, we find $\mathcal{P} \sim \frac{1}{2} - \delta/\alpha$, that is the probability tends to $\frac{1}{2}$, a characteristic feature for asymmetric pulses in the adiabatic limit [23]. The same result can be obtained from equation (14) if we demand $\delta \gg 1$ and use the Stirling asymptotics for the Gamma functions [21] in the phases $\phi_1$ and $\phi_2$ to find

$$\phi_1 - \phi_2 \sim \frac{1}{4\delta^2} \qquad (\delta \gg 1). \tag{17}$$

In contrast, in the limit $\delta \gg \alpha \gg 1$, we find $\mathcal{P} \sim \alpha^2/16\delta^2$; hence the probability vanishes as $\delta^{-2}$ as $\delta$ increases. This latter feature is characteristic for models (e.g., the Rabi model) in which the coupling has sudden changes (discontinuities), such as the sudden termination of the shark pulse at $t_f = \tau$. This feature is illustrated in figure 3 where the transition probability is plotted as a function of $\delta$. The small-$\delta$ asymptotics (14) is seen to provide a good fit to the exact values in its domain of validity. The large-$\delta$ asymptotics (16) describes very accurately the average value of $\mathcal{P}$ in both figures 2 and 3.

## 4. Double-shark pulse

We now turn to the double-shark pulse, for which $t_i = -\tau$ and $t_f = \tau$, as displayed in figure 1(*b*). To find the propagator for this model we separate the interaction into two parts: from $t_i = -\tau$ to $t = 0$, and from $t = 0$ to $t_f = \tau$. The propagator $\mathbf{U}(\tau, 0)$ in the interval $[0, \tau]$ is the same as the one (12) for the shark pulse in the preceding section, $\mathbf{U}(\tau, 0) = \mathcal{U}$. From the symmetry of the Schrödinger equation it can easily be shown that the propagator for the interval $[-\tau, 0]$ is expressed with the help of the Pauli matrix $\sigma_3$ as $\mathbf{U}(0, -\tau) = \sigma_3 \mathcal{U}^T \sigma_3$. The full propagator reads $\mathbf{U}(\tau, -\tau) = \mathbf{U}(\tau, 0)\mathbf{U}(0, -\tau) = \mathcal{U}\sigma_3\mathcal{U}^T\sigma_3$, or explicitly,

$$\mathbf{U}(\tau, -\tau) = \begin{bmatrix} (\Re a - \mathrm{i}\Im b)^2 - (\Re b + \mathrm{i}\Im a)^2 & 2(\Re a \Re b - \Im a \Im b) \\ -2(\Re a \Re b - \Im a \Im b) & (\Re a + \mathrm{i}\Im b)^2 - (\Re b - \mathrm{i}\Im a)^2 \end{bmatrix}. \tag{18}$$

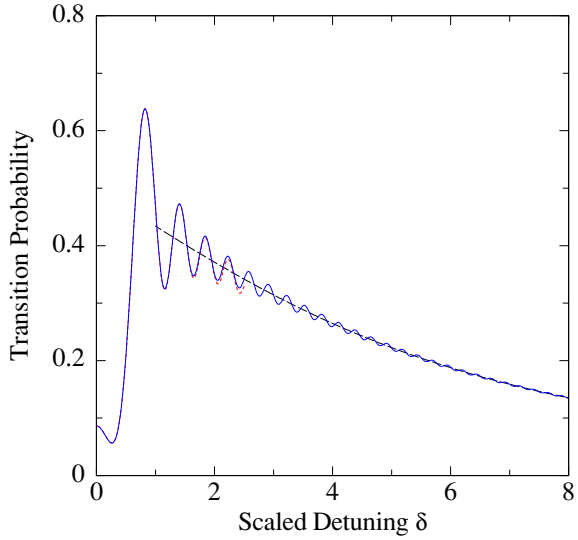


**Figure 3.** The transition probability for a *shark pulse* versus the dimensionless parameter $\delta$ for $\alpha = 15$. The solid curve shows the exact values (13), the short-line dashed curve is asymptotics I (14) and the long-line dashed curve is asymptotics II (16).

The exact transition probability is therefore

$$\mathcal{P} = 4(\Re a \Re b - \Im a \Im b)^2. \tag{19}$$

We point out that the transition probability for this pulse can be derived directly from the general formulae (7) and (10) because the double-shark model is a special case of the general model (3) for $t_i = -\tau$ and $t_f = \tau$. However, the approach we use is more instructive and applicable to the other models that follow.

*Asymptotics I* for $\mathcal{P}$ is derived by using equation (A.3),

$$\mathcal{P} \sim \left[\sqrt{1 - \mathrm{e}^{-2\pi\delta^2}}\cos(\phi_1 + \phi_2) - \frac{2\delta\,\mathrm{e}^{-\pi\delta^2}}{\alpha}\right]^2 \qquad (\alpha \gg 1, \delta). \tag{20}$$

This asymptotics is shown in figure 4 versus $\alpha$ and compared with the exact solution (19). The oscillations in equation (20) have an amplitude which tends to a constant value when $\alpha$ increases; this value is determined by $\delta$.

*Asymptotics II* is obtained by using equations (A.5),

$$\mathcal{P} \sim \frac{\alpha^2}{\alpha^2 + 4\delta^2}\cos^2\left(\frac{\alpha}{2}\sqrt{\alpha^2 + 4\delta^2} + 2\delta^2 \ln\frac{\alpha + \sqrt{\alpha^2 + 4\delta^2}}{2\delta}\right) \qquad (\alpha, \delta \gg 1); \tag{21}$$

hence the oscillations survive even for large $\delta$. The oscillation amplitude is damped versus $\delta$ in a Lorentzian manner. In contrast, it approaches unity as $\alpha$ increases; the same result follows from equation (20) in the limit $\alpha \gg \delta \gg 1$.

The transition probability $\mathcal{P}$ is plotted in figure 5 as a function of $\delta$. An excellent agreement is observed between the asymptotics (20) and (21) and the exact values.

The oscillations that dominate both figures 4 and 5 originate from the presence of two clearly separated parts of the interaction: one for $t < 0$ and another for $t > 0$, which is

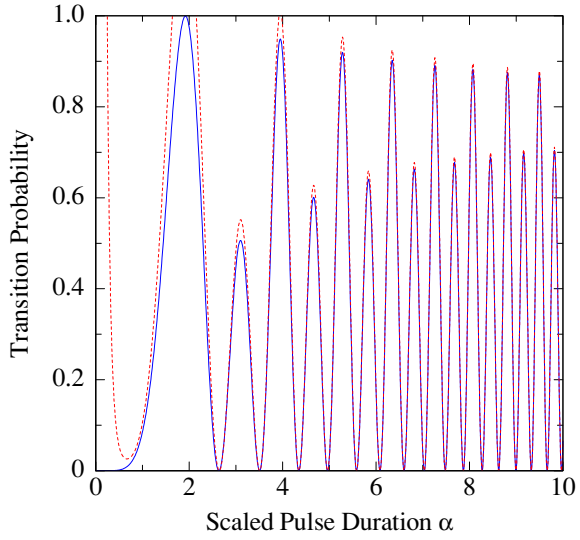


**Figure 4.** The transition probability for a *double-shark pulse* versus the dimensionless parameter $\alpha$ for $\delta = 0.5$. The solid curve shows the exact values (19) and the dashed curve is asymptotics I (20).

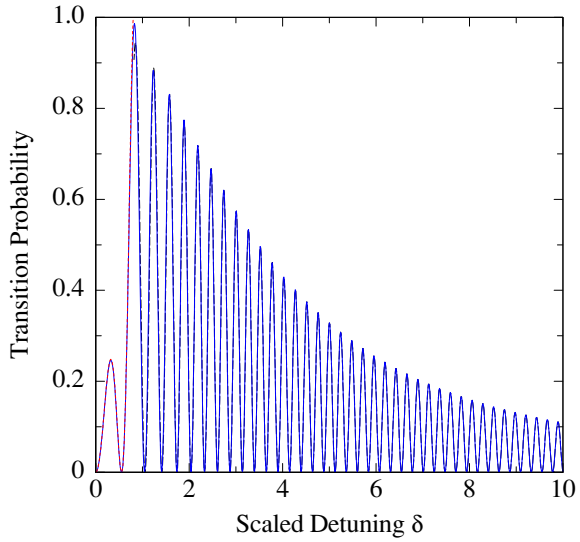


**Figure 5.** The transition probability for a *double-shark pulse* versus the dimensionless parameter $\delta$ for $\alpha = 7$. The solid curve shows the exact values (19), the short-line dashed curve is asymptotics I (20) and the long-line dashed curve is asymptotics II (21) (barely discernible).

reminiscent of Ramsey-type interference. This feature is the physical reason for the presence of considerably more oscillations for the double-shark pulse compared to the shark pulse.

The double-shark pulse is remarkable in another aspect: it has a zero pulse area. Such pulses produce no excitation on resonance ($\delta = 0$). However, they can produce considerable

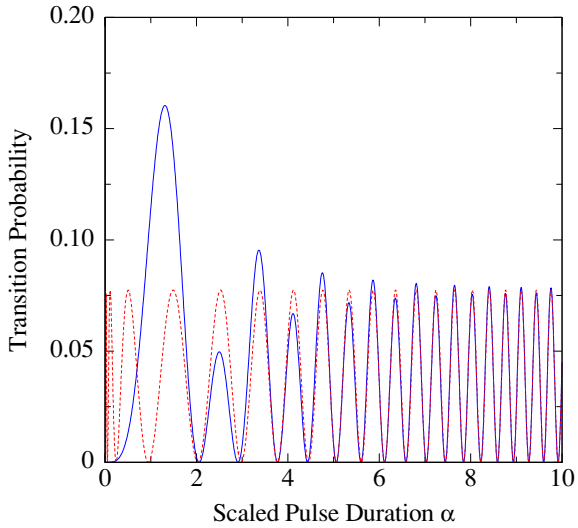


**Figure 6.** The transition probability for a *tent pulse* versus the dimensionless parameter $\alpha$ for $\delta = 1$. The solid curve depicts the exact values (23) and the dashed curve is asymptotics I (24).

excitation off resonance; this problem has been studied in detail elsewhere [24, 25]. Indeed, as visible in both figures 4 and 5, for suitable values of the detuning and the coupling, the transition probability may even reach unity.

## 5. Tent pulse

The tent model is not a special case of the model (3), but has a linear coupling with a positive slope from $t_i = -\tau$ to $t = 0$ and a negative slope (with the same absolute value) from $t = 0$ to $t_f = \tau$, as shown in figure 1(*c*). As in section 4, we exploit the symmetry of the Schrödinger equation to find $\mathbf{U}(0, -\tau) = \mathcal{U}$ and $\mathbf{U}(\tau, 0) = \mathcal{U}^T$. The full propagator is $\mathbf{U}(\tau, -\tau) = \mathcal{U}^T\mathcal{U}$, or explicitly,

$$\mathbf{U}(\tau, -\tau) = \begin{bmatrix} (\Re a - \mathrm{i}\Im b)^2 + (\Re b - \mathrm{i}\Im a)^2 & 2\mathrm{i}(\Re a \Im a - \Re b \Im b) \\ 2\mathrm{i}(\Re a \Im a - \Re b \Im b) & (\Re a + \mathrm{i}\Im b)^2 + (\Re b + \mathrm{i}\Im a)^2 \end{bmatrix}. \tag{22}$$

The exact transition probability reads

$$\mathcal{P} = 4(\Re a \Im a - \Re b \Im b)^2. \tag{23}$$

*Asymptotics I* for $\mathcal{P}$ is derived by using equation (A.3),

$$\mathcal{P} \sim \tfrac{1}{4}\left[(1 - \mathrm{e}^{-\pi\delta^2}) \sin 2\phi_1 - (1 + \mathrm{e}^{-\pi\delta^2}) \sin 2\phi_2\right]^2 \qquad (\alpha \gg 1, \delta). \tag{24}$$

The amplitude of the oscillations in equation (24) is constant versus $\alpha$, as indeed seen in figure 6 for large $\alpha$. A good agreement is observed between the exact probability (23) and its asymptotics (24).

*Asymptotics II* is obtained by using equations (A.5); it reads

$$\mathcal{P} \sim \frac{1}{16\delta^4} \cos^2\left(\frac{\alpha}{2}\sqrt{\alpha^2 + 4\delta^2} + 2\delta^2 \ln\frac{\alpha + \sqrt{\alpha^2 + 4\delta^2}}{2\delta}\right) \qquad (\alpha, \delta \gg 1). \tag{25}$$

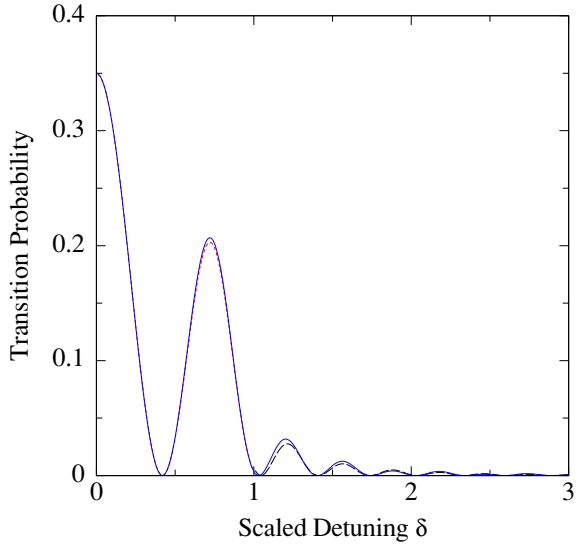


**Figure 7.** The transition probability for a *tent pulse* versus the dimensionless parameter $\delta$ for $\alpha = 7$. The solid curve shows the exact values (23), the short-line dashed curve is asymptotics I (24) and the long-line dashed curve is asymptotics II (25).

The transition probability $\mathcal{P}$ decreases versus $\delta$ as $\delta^{-4}$, i.e. faster than for the shark and double-shark pulses, where $\mathcal{P} \sim \delta^{-2}$. The reason is the absence of a discontinuity in the Hamiltonian for the tent pulse; however, there is a discontinuity in the adiabatic basis, which results in the polynomial $\delta^{-4}$-dependence. The rapid decrease of these oscillations versus $\delta$ is indeed observed in figure 7. A very good agreement between the exact probability (23) and the asymptotics is found once again.

## 6. Zigzag pulse

The zigzag pulse, seen in figure 1(*d*), has a linearly increasing coupling from $t_i = -\tau$ to $t = 0$, with a sudden sign jump at $t = 0$, followed by another linear change from $t = 0$ to $t_f = \tau$. From the symmetry of the Schrödinger equation, as in sections 4 and 5, we find $\mathbf{U}(0, -\tau) = \mathcal{U}$ and $\mathbf{U}(\tau, 0) = \sigma_3 \mathcal{U}^T \sigma_3$. The full propagator is $\mathbf{U}(\tau, -\tau) = \sigma_3 \mathcal{U}^T \sigma_3 \mathcal{U}$; explicitly,

$$\mathbf{U}(\tau, -\tau) = \begin{bmatrix} (\Re a - \mathrm{i}\Im b)^2 - (\Re b - \mathrm{i}\Im a)^2 & 2(\Re a \Re b + \Im a \Im b) \\ -2(\Re a \Re b + \Im a \Im b) & (\Re a + \mathrm{i}\Im b)^2 - (\Re b + \mathrm{i}\Im a)^2 \end{bmatrix}. \tag{26}$$

Hence the exact transition probability reads

$$\mathcal{P} = 4(\Re a \Re b + \Im a \Im b)^2. \tag{27}$$

*Asymptotics I* for $\mathcal{P}$ is obtained by using equation (A.3),

$$\mathcal{P} \sim \left\{ \sqrt{1 - \mathrm{e}^{-2\pi\delta^2}} \cos(\phi_1 - \phi_2) + \frac{\delta}{\alpha} \left[ (1 - \mathrm{e}^{-\pi\delta^2}) \cos 2\phi_1 - (1 + \mathrm{e}^{-\pi\delta^2}) \cos 2\phi_2 \right] \right\}^2 \qquad (\alpha \gg 1, \delta). \tag{28}$$

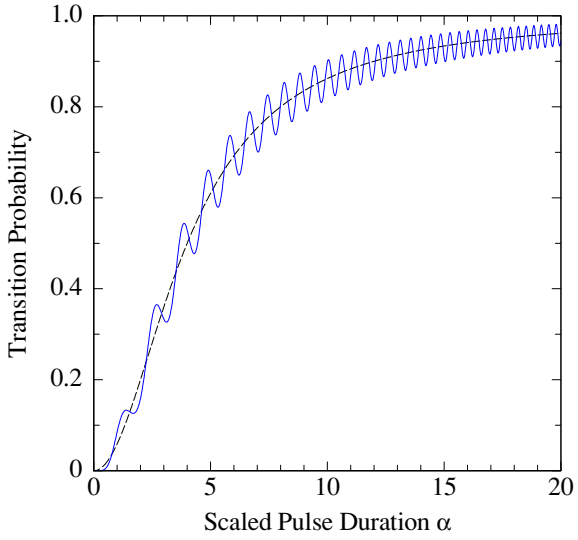


**Figure 8.** The transition probability for a *zigzag pulse* versus the dimensionless parameter $\alpha$ for $\delta = 2$. The solid curve is the exact probability (27) and the long-line dashed curve is asymptotics II (29).

*Asymptotics II* is obtained by using equations (A.5); it reads

$$\mathcal{P} \sim \frac{\alpha^2}{\alpha^2 + 4\delta^2} \qquad (\alpha, \delta \gg 1). \tag{29}$$

The transition probability $\mathcal{P}$ is plotted in figure 8 as a function of $\alpha$; it exhibits damped oscillations and tends to a value that depends on $\delta$; for sufficiently large $\delta$ this value is close to unity. The asymptotics (29) describes very accurately the mean value of $\mathcal{P}$.

Figure 9 shows $\mathcal{P}$ as a function of $\delta$. The asymptotics (28) and (29) match very well the exact solution (27) once again. The Lorentzian decrease of $\mathcal{P}$ versus $\delta$ is a consequence of the discontinuity at time $t = 0$.

There is an interesting feature of this model, visible in equation (29): when $\alpha \gg \delta \gg 1$ we have $\mathcal{P} \to 1$, which implies CPI. This CPI is caused by a $\delta$-function-shaped nonadiabatic coupling in the adiabatic basis as discussed elsewhere [24, 25]; it is encountered here too. A nearly complete inversion is seen in figure 9 for $\delta \approx 1$ to 3. For this CPI, both conditions $\delta \gg 1$ and $\alpha \gg \delta$ are essential; because $\alpha$ is only moderately large ($\alpha = 15$), these conditions are satisfied approximately only in a limited range of $\delta$.

## 7. Adiabatic solution

We shall now derive the adiabatic solution for the general model (3) and the other four special models above. The adiabatic states $\varphi_+(t)$ and $\varphi_-(t)$ are defined as the eigenstates of the Hamiltonian (2), $\mathbf{H}(t)\varphi_\pm(t) = \hbar\epsilon_\pm(t)\varphi_\pm(t)$, with eigenvalues $\hbar\epsilon_\pm(t) = \pm\hbar\epsilon(t)$, where

$$\epsilon(t) = \tfrac{1}{2}\sqrt{\Omega^2(t) + \Delta^2(t)}. \tag{30}$$

The amplitudes of the adiabatic states $\mathbf{A}(t) = [A_+(t), A_-(t)]^T$ are connected with the original ones $\mathbf{C}(t)$ via the rotation matrix (5) as $\mathbf{C}(t) = \mathbf{R}(\theta(t))\mathbf{A}(t)$, where $\theta(t) = \frac{1}{2}\arctan[\Omega(t)/\Delta]$.

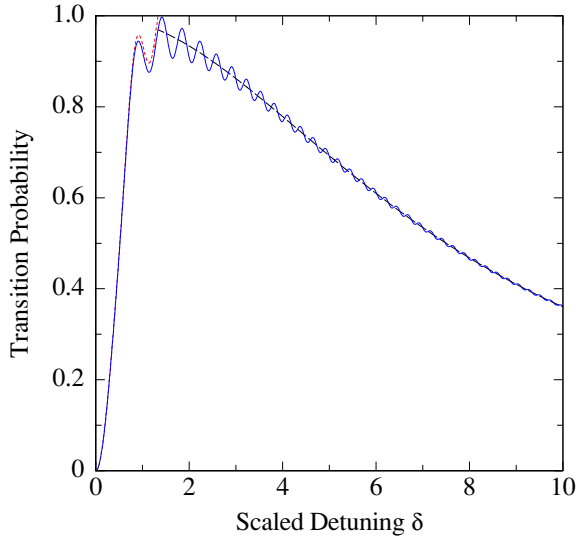


**Figure 9.** The transition probability for a *zigzag pulse* versus the dimensionless parameter $\delta$ for $\alpha = 15$. The solid curve shows the exact probability (27), the short-line dashed curve is asymptotics I (28) and the long-line dashed curve is asymptotics II (29).

The Schrödinger equation in the adiabatic basis reads

$$\mathrm{i}\hbar\frac{\mathrm{d}}{\mathrm{d}t}\mathbf{A}(t) = \mathbf{H}_A(t)\mathbf{A}(t), \tag{31}$$

where

$$\mathbf{H}_A = \hbar\begin{bmatrix}\epsilon_- & -\mathrm{i}\dot{\theta}\\ \mathrm{i}\dot{\theta} & \epsilon_+\end{bmatrix}. \tag{32}$$

If $|\dot{\theta}| \ll \epsilon$, then the evolution is adiabatic and the solution for the propagator in the adiabatic basis from time $t_i$ to time $t_f$ reads

$$\mathbf{U}_A(t_f, t_i) = \begin{bmatrix}\mathrm{e}^{\mathrm{i}\zeta} & 0\\ 0 & \mathrm{e}^{-\mathrm{i}\zeta}\end{bmatrix}, \tag{33}$$

where

$$\zeta = \int_{t_i}^{t_f}\epsilon(t)\,\mathrm{d}t = \left[\frac{1}{4}\alpha\sqrt{4\delta^2+\alpha^2} + \delta^2\ln(\alpha+\sqrt{4\delta^2+\alpha^2})\right]_{\alpha_i}^{\alpha_f}. \tag{34}$$

The full propagator in the original basis for the model (3) reads

$$\mathbf{U}_{\mathrm{adiab}}(t_f, t_i) = \mathbf{R}(\theta_f)\mathbf{U}_A(t_f, t_i)\mathbf{R}(-\theta_i), \tag{35}$$

with $\theta_{i,f} = \theta(t_{i,f})$. The adiabatic transition probability in the original basis is

$$\mathcal{P}_{\mathrm{adiab}} = \frac{1}{2} - \frac{1}{2}\frac{\Delta^2}{\epsilon(t_i)\epsilon(t_f)} - \frac{1}{2}\frac{\Omega(t_i)\Omega(t_f)}{\epsilon(t_i)\epsilon(t_f)}\cos 2\zeta. \tag{36}$$

*Shark model* ($t_i = 0$). The adiabatic transition probability of this model reads

$$\mathcal{P}_{\mathrm{adiab}} = \frac{1}{2} - \frac{\delta}{\sqrt{\alpha^2+4\delta^2}}, \tag{37}$$

which coincides with asymptotics II (16).

*Double-shark model* ($t_i = -t_f$). For this model we find

$$\mathcal{P}_{\text{adiab}} = \frac{\alpha^2}{\alpha^2 + 4\delta^2} \cos^2 \zeta, \tag{38}$$

which is equal to asymptotics II (21).

*Tent model.* For this model, the adiabatic solution reads

$$\mathcal{P}_{\text{adiab}} = 0. \tag{39}$$

*Zigzag model.* In this model we have to account for the jump in $\Omega(t)$ at $t = 0$, see figure 1(*d*). This discontinuity causes a delta-function behavior of the nonadiabatic coupling $\dot{\theta}(t)$ in the same point $t = 0$, which in turn causes a transition between the adiabatic states with an area equal to the area of the delta-function feature, which is $\theta_0 = \arctan(\alpha/2\delta)$. The propagator that describes this transition in the adiabatic basis is $\mathbf{R}(\theta_0)$. Hence the propagator $\mathbf{U}_A(t_f, t_i)$ in equation (35) is split by this transition and should be replaced by the sandwich $\mathbf{U}_A(t_f, 0)\mathbf{R}(\theta_0)\mathbf{U}_A(0, t_i)$. The propagator in the original basis reads

$$\mathbf{U}_{\text{adiab}}(t_f, t_i) = \mathbf{R}(\theta_f)\mathbf{U}_A(t_f, 0)\mathbf{R}(\theta_0)\mathbf{U}_A(0, t_i)\mathbf{R}(-\theta_i). \tag{40}$$

with $\theta_f = \theta_i = 0$ now. After simple algebra the transition probability is obtained as

$$\mathcal{P}_{\text{adiab}} = \frac{\alpha^2}{\alpha^2 + 4\delta^2}, \tag{41}$$

which is the same as asymptotics II (29).

It is evident from the above results that the adiabatic solution coincides with asymptotics II, which required $\alpha, \delta \gg 1$. A closer inspection of the adiabatic condition reveals that the adiabatic condition $|\dot{\theta}(t)| \ll \epsilon(t)$ translates into $2\delta \ll (\beta^2 t^2 + 4\delta^2)^{3/2}$. We note that this condition is satisfied least well for $t = 0$; there the adiabatic condition reduces to

$$4\delta^2 \gg 1. \tag{42}$$

Hence, even only a moderately large $\delta$ ($\delta \gtrsim 1$) is sufficient to enforce adiabatic evolution. This feature explains the accuracy of asymptotics II well beyond its formal range of validity ($\alpha, \delta \gg 1$) observed in figures 2 (where $\delta = 1.5$) and 8 (where $\delta = 2$), and also in the small-$\delta$ ranges in figures 3, 5, 7 and 9.

The apparent discrepancy for the tent model, where the adiabatic solution produces a null probability, indicates that the respective asymptotics II (25) is of superadiabatic nature.

## 8. Conclusions

In this paper, we have presented an analytically exactly soluble two-state model, in which the Rabi frequency is a linear function of time with a finite duration and the detuning is constant. This model is reminiscent of the famous Landau–Zener model where, however, the Rabi frequency is constant and the detuning is linear. Because the Hamiltonians, and the propagators, for these two models are related to each other by a basis rotation at an angle of $\pi/4$, we have used the known LZ solution to derive the propagator for the present model. The exact evolution matrix in the general case is expressed in terms of sums of products of parabolic cylinder functions $D_\nu(z)$.

Several approximations in terms of simpler functions have been derived based on (i) the large-argument asymptotics of $D_\nu(z)$, and (ii) the large-argument-and-large-order asymptotics of $D_\nu(z)$. The former of these corresponds to a peak Rabi frequency much larger than the

detuning and the inverse time duration $1/\tau$, whereas the latter requires that the peak Rabi frequency and the detuning are simultaneously much larger than $1/\tau$. These approximations have been applied to several physically distinct models. The *shark pulse* is an example of an asymmetric pulse. The antisymmetric *double-shark pulse* is an example of a pulse with zero area, and also a pulse composed of two separated parts, similar to a Ramsey interferometer. The *tent model* is an example of a symmetric pulse, which experiences complete population return in the adiabatic limit. Finally, the *zigzag model* has a sign jump in the coupling at $t = 0$; it produces complete population inversion for sufficiently large Rabi frequency and detuning, despite its overall zero pulse area. All derived asymptotics fit very accurately the exact values in the relevant domains.

To conclude, the pulse shapes described in this work can be realized in the lab with relative ease, for example, in nuclear magnetic resonance [1] and coherent atomic excitation [29, 30]. For instance, laser pulses of such shapes can be produced by pulse shaping of femtosecond pulses [29] or by acousto-optic modulation of microsecond pulses [30].

## Acknowledgments

This work has been supported by the European Commission's projects CAMEL, EMALI and FASTQUAST and the Bulgarian National Science Fund Grants VU-205/06 and VU-301/07.

## Appendix. Relevant properties of the parabolic cylinder function

The parabolic cylinder (Weber) function $D_\nu(z)$ [21] is a solution of the Weber equation

$$\frac{\mathrm{d}^2}{\mathrm{d}z^2} D_\nu(z) + \left(\nu + \frac{1}{2} - \frac{1}{4}z^2\right) D_\nu(z) = 0. \tag{A.1}$$

The power series expansion is relevant for small $|z|$ and has the form [26]

$$D_\nu(z) = 2^{\nu/2}\pi^{1/2}\,\mathrm{e}^{z^2/4} \sum_{n=0}^{\infty} \frac{(-z\sqrt{2})^n}{n!\Gamma\left[\frac{1}{2}(1-n-\nu)\right]}. \tag{A.2}$$

The large-argument asymptotic expansions are relevant when $|z| \gg 1, |\nu|$. The basic one is [21]

$$D_\nu(z) \sim z^\nu\,\mathrm{e}^{-\frac{1}{4}z^2}\left[\sum_{n=0}^{N} \frac{\left(-\frac{1}{2}\nu\right)_n \left(\frac{1}{2}-\frac{1}{2}\nu\right)_n}{n!\left(-\frac{1}{2}z^2\right)_n} + \mathcal{O}(|z^2|^{-N-1})\right],$$
$$(|z| \to \infty, |\arg z| < 3\pi/4, \nu \text{ fixed}), \tag{A.3}$$

where $(a)_n = \Gamma(a+n)/\Gamma(a)$. The asymptotics for other values of $\arg z$ is found by using the connection formula [21]

$$D_\nu(z) = \mathrm{e}^{\mathrm{i}\pi\nu} D_\nu(-z) + \frac{\sqrt{2\pi}}{\Gamma(-\nu)}\,\mathrm{e}^{\mathrm{i}(\nu+1)\pi/2} D_{-1-\nu}(-\mathrm{i}z). \tag{A.4}$$

The existence of different asymptotic expansions for different values of $\arg z$ is a manifestation of the Stokes phenomenon [27, 28].

The large-argument-and-large-order asymptotic expansions are relevant when both $|z|$ and $|\nu|$ are simultaneously much larger than unity [22]. These expansions are generally more complicated than the asymptotics (A.3). For the particular functions involved in the present models the asymptotic expansions can be derived from the general results of Olver [22]; their

leading terms are [20]

$$D_{i\delta^2}(\alpha\, e^{-i\pi/4}) \sim \cos\theta\, e^{\pi\delta^2/4+i\eta}, \tag{A.5a}$$

$$D_{-i\delta^2}(\alpha\, e^{i\pi/4}) \sim \cos\theta\, e^{\pi\delta^2/4-i\eta}, \tag{A.5b}$$

$$D_{-1-i\delta^2}(\alpha\, e^{i\pi/4}) \sim \frac{\sin\theta}{\delta}\, e^{\pi\delta^2/4-i\eta-i\pi/4}, \tag{A.5c}$$

$$D_{-1+i\delta^2}(\alpha\, e^{-i\pi/4}) \sim \frac{\sin\theta}{\delta}\, e^{\pi\delta^2/4+i\eta+i\pi/4}, \tag{A.5d}$$

$$D_{i\delta^2}(\alpha\, e^{3i\pi/4}) \sim \cos\theta\, e^{-3\pi\delta^2/4+i\eta} + \frac{\delta\sqrt{2\pi}\,\sin\theta}{\Gamma(1-i\delta^2)}\, e^{-\pi\delta^2/4-i\eta-i\pi/4}, \tag{A.5e}$$

$$D_{-1+i\delta^2}(\alpha\, e^{3i\pi/4}) \sim \frac{\sin\theta}{\delta}\, e^{-3\pi\delta^2/4+i\eta-3i\pi/4} + \frac{\sqrt{2\pi}\,\cos\theta}{\Gamma(1-i\delta^2)} e^{-\pi\delta^2/4-i\eta}, \tag{A.5f}$$

where $\alpha$ and $\delta$ are assumed positive and large ($\alpha \to \infty, \delta \to \infty, \alpha/\delta$ is arbitrary), $\theta = \frac{1}{2}\arctan(2\delta/\alpha)$, and

$$\eta = \frac{1}{2}\alpha\sqrt{\alpha^2+4\delta^2} - \frac{1}{2}\delta^2 + \delta^2 \ln\left[\frac{1}{2}(\alpha + \sqrt{\alpha^2+4\delta^2})\right], \tag{A.6}$$

The first four expansions, for phases of the arguments equal to $\pi/4$, are derived [20] directly from Olver's results [22]. The last two asymptotics, for phases of the argument equal to $3\pi/4$, are obtained from equations (A.5*a*)–(A.5*d*) by using the connection formula (A.4).

## References


[1] Abraham A 1961 *The Principles of Nuclear Magnetism* (Oxford: Clarendon)
Slichter C P 1990 *Principles of Magnetic Resonance* (Berlin: Springer)
[2] Nikitin E E and Umanskii S Y 1984 *Theory of Slow Atomic Collisions* (Berlin: Springer)
[3] Shore B W 1990 *The Theory of Coherent Atomic Excitation* (New York: Wiley)
[4] Nielsen M A and Chuang I L 2000 *Quantum Computation and Quantum Information* (Cambridge: Cambridge University Press)
Bouwmeester D, Ekert A and Zeilinger A 2000 *The Physics of Quantum Information: Quantum Cryptography, Quantum Teleportation, Quantum Computation* (Berlin: Springer)
[5] Rabi II 1937 *Phys. Rev.* **51** 652
[6] Landau L D 1932 *Phys. Z. Sowjetunion* **2** 46
Zener C 1932 *Proc. R. Soc. Lond.* A **137** 696
[7] Rosen N and Zener C 1932 *Phys. Rev.* **40** 502
[8] Allen L and Eberly J H 1987 *Optical Resonance and Two-Level Atoms* (New York: Dover)
[9] Hioe F T 1984 *Phys. Rev.* A **30** 2100
[10] Bambini A and Berman P R 1981 *Phys. Rev.* A **23** 2496
[11] Demkov Y N and Kunike M 1969 *Vestn. Leningr. Univ. Fiz. Khim.* **16** 39
Hioe F T and Carroll C E 1985 *Phys. Rev.* A **32** 1541
Zakrzewski J 1985 *Phys. Rev.* A **32** 3748
[12] Demkov Y N 1964 *Sov. Phys.—JETP* **18** 138
[13] Nikitin E E 1962 *Opt. Spectrosc.* **13** 431
[14] Carroll C E and Hioe F T 1986 *J. Phys. A: Math. Gen.* **19** 3579
[15] Carroll C E and Hioe F T 1990 *Phys. Rev.* A **41** 2835
[16] Vitanov N V, Halfmann T, Shore B W and Bergmann K 2001 *Ann. Rev. Phys. Chem.* **52** 763
[17] Dykhne A M 1960 *Sov. Phys.—JETP* **11** 411
Dykhne A M 1962 *Sov. Phys.—JETP* **14** 941
Davis J P and Pechukas P 1976 *J. Chem. Phys.* **64** 3129
[18] Vitanov N V and Stenholm S 1997 *Phys. Rev.* A **55** 2982
[19] Yatsenko L P, Guérin S and Jauslin H R 2004 *Phys. Rev.* A **70** 043402

[20] Vitanov N V and Garraway B M 1996 *Phys. Rev.* A **53** 4288
[21] Erdélyi A, Magnus W, Oberhettinger F and Tricomi F G 1953 *Higher Transcendental Functions* (New York: McGraw-Hill)
[22] Olver F W J 1959 *J. Res. Natl Bur. Stand.* B **63** 131
[23] Vitanov N V 1994 *J. Phys. B: At. Mol. Opt. Phys.* **27** 1351
Vitanov N V and Knight P L 1995 *J. Phys. B: At. Mol. Opt. Phys.* **28** 1905
[24] Vasilev G S and Vitanov N V 2006 *Phys. Rev.* A **73** 023416
[25] Vitanov N V 2007 *New J. Phys* **9** 58
[26] Abadir K M 1993 *J. Phys. A: Math. Gen.* **26** 4059
[27] Dingle R B 1973 *Asymptotic Expansions: Their Derivation and Interpretation* (London: Academic)
[28] Olver F W J 1974 *Asymptotics and Special Functions* (London: Academic)
[29] Diels J-C and Rudolph W 1996 *Ultrashort Laser Pulse Phenomena: Fundamentals, Techniques, and Applications on a Femtosecond Time Scale* (San Diego, CA: Academic)
Wollenhaupt M, Engel V and Baumert T 2005 *Annu. Rev. Phys. Chem.* **56** 25
Brixner T, Pfeifer T, Gerber G, Wollenhaupt M and Baumert T 2005 *Femtosecond Laser Spectroscopy* ed P Hannaford (New York: Springer) chapter 9
[30] Weitz M, Young B C and Chu S 1994 *Phys. Rev. Lett.* **73** 2563